Influence of Segmentation and Ambipolar Diffusion on MHD Nonequilibrium Boundary Layers

E. D. Doss,* H. A. Dwyer,† and M. A. Hoffman‡
University of California, Davis, Calif.

The compressible laminar and turbulent boundary-layer equations representing the flow of cesium seeded argon plasma over successive segments of the cathode wall of an MHD channel were investigated and solved for both finite and infinite rates of reaction. The equations solved include the electron energy and the electron continuity equations as well as the usual global boundary-layer equations. The effects of finite rates of reaction and ambipolar diffusion are considered, and the inner boundary conditions for both the electron energy and the electron continuity equations are obtained by investigating a sheath analysis. The governing equations are solved using a finite-difference scheme without introducing a local similarity assumption. The finite rate results are considerably different from the infinite rate ones. The main reason is the ambipolar diffusion which depletes the electrons near the wall. No special problems have been found in the solution of the turbulent flow equations. This is due to the high mobility of electrons.

Introduction

QUITE recently the subject of MHD has received renewed attention in the engineering scientific literature. The main recent interest in MHD is for direct conversion of the thermal and kinetic energy of a flowing plasma into electrical energy. To do this, one must understand the MHD boundary layer occurring in the internal flow of a plasma over the electrode and insulator surfaces in order to predict the performance characteristics of the channel.

MHD boundary-layer investigations have been considered by several authors. The treatment of the governing equations among the different investigators differs primarily in the method of solution and the interaction between the plasma and the wall. Kerrebrock[1,2] carried out some early attempts to analyze the MHD boundary layers. The electron energy equation was neglected and an equilibrium plasma was assumed. Later Hale and Kerrebrock[3] allowed for the electrical conductivity to depend on the current density. Oates[4] determined the electron temperature on the basis of a simple balance between the energy gained in the electric field and the energy lost by collision, rather than the complete electron equation. (Local similarity was assumed in all previous work.)

Sherman and Reshotko[5,6] considered a steady laminar two-dimensional boundary layer for cesium seeded argon. The electron energy equation was considered in their early work[5] where the electron number density was determined by the Saha equation evaluated at the local electron temperature. Sherman et al.[6] next allowed for finite rate of ionization and recombination. Therefore, a separate equation for the electron continuity equation was needed. However, ambipolar diffusion was neglected in their analysis, which could be quite important. The equations were solved using a finite-difference scheme. Brown[7] found theoretically and experimentally the electron number density and the electron temperature over a cooled flat plate with no magnetic field and where the surface was electrically floating and nonemitting. Finite rates of reaction and ambipolar diffusion were included in his analysis. A mixed sheath region was considered and a local similarity approach was also used. Cott[8] studied the boundary layer over the B-wall (insulator) of an MHD accelerator, and a transition region was assumed in his sheath analysis.

All the work mentioned so far has been for laminar flow. Teno et al.[9,10] considered the growth of the boundary layer in an MHD generator with the emphasis on the boundary-layer separation. An integral method was used to analyze the electrode boundary layer but their analysis is approximate, semi-empirical and contains many assumptions. High and Felderman[11] extended the work of Cott[8] for the turbulent flow using the eddy viscosity approach and with the assumption of a collisionless sheath.

Demetriades and Argyropoulos[12,13] discussed most of the practical problems of an MHD power generator. They indicated that there are two problems that have to be solved. First, the "gas dynamic problem," if the current distribution is known, and the "electrical problem" if the values of the gas dynamic distributions are given. These two solutions can then be used to get the solution of the "coupled" problem using an iterative procedure.

The present investigation will extend and combine some of the previous work. For example, the work of Sherman and Reshotko[5,6] will be extended over many electrode pairs to show the influence of segmentation, and the ambipolar diffusion. Also, a turbulent flow solution will be carried out. However, this work will be limited to the study of the gas dynamic problem where the external current density distribution is specified. First, the formulation of the problem and the governing equations are discussed, and the sheath analysis is presented. The finite-difference procedure is then formulated. Finally, some interesting results for the finite and infinite rates of reaction are presented and discussed.

Analysis

1. Assumptions

The following assumptions are introduced to simplify the governing equations: 1) steady flow; 2) no induced magnetic field; 3) plasma consists of main gas, seed atoms, and singly ionized seeds; 4) no continuum radiation loss; 5) collisionless sheath; 6) the electron density is determined by the Saha relation evaluated at the local electron temperature for the infinite

Received March 12, 1973; revision received September 20, 1973.
Index categories: Plasma Dynamics and MHD; Boundary Layers and Convective Heat Transfer—Laminar; Boundary Layers and Convective Heat Transfer—Turbulent.

* Presently associated with STD Research Corporation, Arcadia, Calif.
† Associate Professor, Mechanical Engineering Department. Member AIAA.
‡ Professor, Mechanical Engineering Department.

rates of reaction case; 7) ion slip is neglected in Ohm's law but is included in the other governing equations for finite rates of reaction; 8) the process of ionization for finite rates occurs as a result of collisions between electrons and neutrals, while the recombination process is predominantly of the three body type; and 9) surface emission is only due to diffuse thermionic emission.

2. Governing Equations

The general equations for a multicomponent nonequilibrium gas are given in Ref. 14. For the two-dimensional flow, using the boundary-layer assumptions and the eddy viscosity approach to relate the fluctuating quantities to the mean flow quantities, the boundary-layer equations are given as follows[15]:

Global Continuity

$$(\partial/\partial x)(\rho u)+(\partial/\partial y)(\overline{\rho v}) = 0 \tag{1}$$

Global Momentum

$$\rho u\frac{\partial u}{\partial x} + \overline{\rho v}\frac{\partial u}{\partial y} = \rho_\infty u_\infty \frac{du_\infty}{dx} + \frac{\partial}{\partial y}\left[(\mu+\varepsilon)\frac{\partial u}{\partial y}\right] \tag{2}$$

Global Energy

$$\rho u\frac{\partial h}{\partial x} + \overline{\rho v}\frac{\partial h}{\partial y} = u\frac{dp}{dx} + (\mu+\varepsilon)\left(\frac{\partial u}{\partial y}\right)^2 + \frac{j^2}{\sigma} - \frac{\partial}{\partial y}(q_y) - \dot{n}_e \varepsilon_1 \tag{3}$$

where

$$-\frac{\partial}{\partial y}(q_y) = \frac{\partial}{\partial y}\left[\left(\frac{\mu}{P}+\frac{\varepsilon}{P_t}\right)\frac{\partial h}{\partial y} + \frac{k_e}{C_{v,e}}\frac{\partial h_e}{\partial y} + \frac{5}{2}KT_e\frac{j_y}{e}\right] + \frac{\partial}{\partial y}\left[\frac{\mu}{S}(h_e+h)\frac{\partial C_e(1+T_e/T)}{\partial y} + \frac{\varepsilon}{S_t}(h_e+h)\frac{\partial C_e}{\partial y}\right] \tag{4}$$

Electron Energy

$$\rho_e u\frac{\partial T_e}{\partial x} + \rho_e v\frac{\partial T_e}{\partial y} = \frac{2}{3}C_e T_e\left(u\frac{\partial \rho}{\partial x} + v\frac{\partial \rho}{\partial y}\right) + \frac{1}{C_{v,e}}\frac{j^2}{\sigma} + \frac{1}{C_{v,e}}3\rho_e K(T-T_e)\sum_s \frac{\nu_{es}}{m_s} - \frac{1}{C_{v,e}}\frac{\partial}{\partial y}(q_{ey}) - \dot{n}_e\left(\frac{2\varepsilon_I}{3K} + T_e\right) \tag{5}$$

where

$$-\frac{1}{C_{v,e}}\frac{\partial}{\partial y}(q_{ey}) = \frac{\partial}{\partial y}\left[\frac{k_e}{C_{v,e}}\frac{\partial T_e}{\partial y} + \frac{1}{C_{v,e}}\frac{5}{2}KT_e\frac{j_y}{e}\right] + \frac{\partial}{\partial y}\left[\frac{\mu}{S}T_e\frac{\partial C_e(1+T_e/T)}{\partial y} + \frac{\varepsilon}{S_t}T_e\frac{\partial C_e}{\partial y}\right] \tag{6}$$

Electron Continuity

$$\rho u\frac{\partial C_e}{\partial x} + \overline{\rho v}\frac{\partial C_e}{\partial y} = \frac{\partial}{\partial y}\left[\frac{\mu}{S}\frac{\partial C_e(1+T_e/T)}{\partial y} + \frac{\varepsilon}{S_t}\frac{\partial C_e}{\partial y}\right] + \dot{\rho}_e \tag{7}$$

In the previous equations, the following notation has been used: x, y are the position coordinates; u, v are the corresponding components of velocity; p is the static pressure; ρ is the mass density; h is the static enthalpy, T is the static temperature; μ, ε are the dynamic and eddy viscosities; k is the thermal conductivity; $\dot{n}_e$ is the net rate of electron production; q_y is the heat flux; j, E are the current density and electric field; σ is electrical conductivity; ε_I is the ionization energy of seed; $C_e = n_e m_e/\rho$ is the electron mass concentration; m_s is the mass of species s; P, S are the Prandtl and Schmidt numbers; ν_{es} is the electron collision frequency; $C_{v,e} = \frac{3}{2}(K/m_e)$ is the specific heat of electrons, where K is the Boltzmann constant and $\overline{\rho v} = \bar{\rho}\bar{v} + \overline{\rho' v'}$ where the second term on the right-hand side is the time average of the fluctuating quantities. The subscript e refers to electrons, s is the species, t is the turbulent, and ∞ is the freestream quantity.

Maxwell's Relations and Ohm's Law

In order to relate the electrical variables to each other as well as to the fluid dynamics of the problem, the Maxwell's relations and Ohm's law are introduced. While the solution of these equations has been completed for a very simplified model, it is difficult to solve for the general case. At this point the assumptions of Sherman and Reshotko[5,6] will be adopted, where the fact that the boundary-layer thickness is small compared to the electrode, and insulator segment lengths have been used to assume the following: over the electrode $j_y = j_{y_\infty}$, $E_x = 0$, while over the insulator $j_y = 0$ and $E_x = E_{x_\infty}$. Using these assumptions together with the generalized Ohm's law (with no ion slip), the quantities $j \cdot E$ and j^2/σ appearing in the boundary-layer equations can be expressed[5,6] in terms of j_{y_∞} and E_{x_∞}.

The finite rate of production of electrons is obtained using the expression[16]

$$\dot{n}_e = \alpha_{\text{rec}} n_e(n_{e_s}{}^2 - n_e{}^2) \tag{8}$$

where α_{rec} is the Hinnov-Hirschberg recombination coefficient given by $\alpha_{\text{rec}} = 3.4\ 10^{-34}(T_e/1000)^{-9/2}\ \text{m}^6/\text{sec}$ and n_{e_s} is the equilibrium electron number density calculated from the Saha equation.

3. Boundary Conditions

a. Freestream boundary conditions

$$u(x,\infty) = u_\infty(x),\quad T(x,\infty) = T_\infty(x),\quad T_e(x,\infty) = T_{e_\infty}(x),\quad n_e(x,\infty) = n_{e_\infty}(x) \tag{9}$$

where the electron number density is assumed to take the equilibrium Saha value in the freestream.

b. Wall boundary conditions

$$u(x,0) = 0,\quad v(x,0) = 0 \quad \text{and} \quad T(x,0) = T_w(0) \quad \text{or} \quad q(x,0) = q_w(0) \tag{10}$$

c. Sheath analysis

To specify the inner boundary condition on the electron temperature T_e and the number density n_e, a study of the plasma sheath must be considered. A free molecular collisionless sheath region is assumed to exist near the wall which is matched to the continuum regime at the sheath edge. The validity of such an assumption has been discussed in Refs. 6, 8, 11, 17. The plasma sheath analysis in Ref. 17 will be adopted here with the allowance for ambipolar diffusion.

In order to obtain the wall boundary condition for the electron energy equation, the conservation of current should be satisfied everywhere

$$j_{y_\infty} = \left[\frac{n_{e_w} e\langle V_e\rangle}{4}\exp\frac{-e\Delta\phi}{KT_{e_w}} - i\right] - n_{i_w} e\langle V_i\rangle \tag{11}$$

where T_{e_w} is the electron temperature at the sheath edge, n_e, n_i are the number densities of electrons and ions ($n_e = n_i$ at the sheath edge), $\Delta\phi$ is the sheath voltage drop, and i is the surface emission current. $\langle V_e\rangle$ and $\langle V_i\rangle$ are the mean electron and ion velocities at the sheath edge.

For the electron energy flux, we obtain

$$\left[k_e\left(\frac{\partial T_e}{\partial y}\right)\right]_w + C_{v,e}\left[\frac{\mu}{S}T_e\frac{\partial C_e(1+T_e/T)}{\partial y}\right]_w + \frac{5}{2}KT_{e_w}\frac{(j_{ey})}{e} = \left[\frac{n_e\langle V_e\rangle}{4}\exp\left(\frac{-e\Delta\phi}{KT_{e_w}}\right)\right](2KT_{e_w} + e\Delta\phi) - \frac{i}{e}(2KT_w + e|\Delta\phi|) \tag{12}$$

where j_{ey} is the electron current density which is given by the first two terms between the brackets on the right-hand side of Eq. (11). From Eqs. (11) and (12), the sheath voltage drop $\Delta\phi$ and the boundary condition on T_{e_w} can be obtained.

For the electron continuity wall boundary condition, the conservation of ions through the sheath is used

$$\frac{1}{m_e}\left[\frac{\mu}{S}\frac{\partial C_e(1+T_e/T)}{\partial y}\right]_w = n_{i_w}\langle V_i\rangle \tag{13}$$

Method of Solution

1. Transformation of Coordinates

Solving the boundary-layer equations can be considerably simplified by transforming the dependent and independent

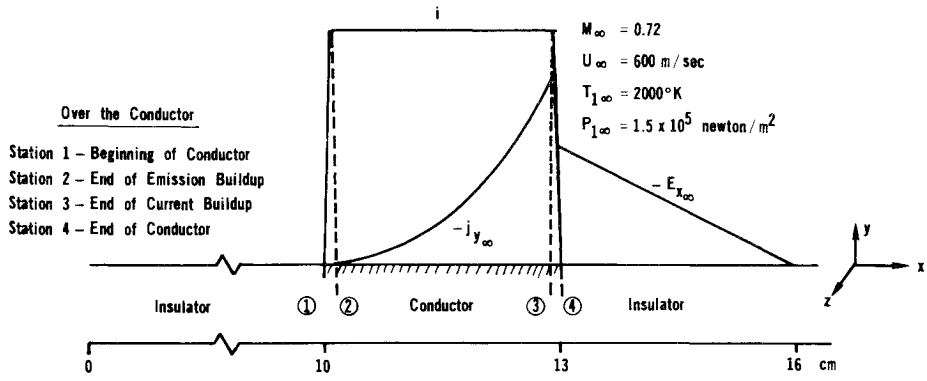

Fig. 1 Conditions imposed on the channel.

variables. The main objectives of the transformations are: 1) limit the boundary-layer growth due to compressibility and locate approximately the edge of the boundary layer; 2) decrease the changes and gradients of the dependent variables; and 3) remove the leading edge singularities and starting difficulties. The transformations used in the present work are

$$\xi(x) = \int_0^x (\rho\mu)_r u_\infty \, dx, \qquad \eta(x, y) = \frac{u_\infty}{(2\xi)^{1/2}} \int_0^x \rho \, dy \qquad (14)$$

where r denotes a reference value which has been evaluated at the surface.

2. External Conditions

In the present work, a constant velocity channel flow is considered. The one-dimensional inviscid flow solution for such a case is given with some simplifications in Ref. 18. Since radiation escape is neglected, and for low current density values, it is assumed that $T_{e_\infty}(x) = T_\infty(x)$.

In the absence of good information about the external current density and electric field distributions, j_{y_∞} has been assumed to take a parabolic variation over the electrode. Determination of E_{x_∞} has been calculated using Ohm's law for the average quantities. As a first approximation, the variation of E_{x_∞} over the insulator is assumed linear. Different distributions with higher powers in their variation were also examined and no significant changes in the results were observed.

3. Initial Conditions

a. Laminar flow

The initial velocity profile is taken as the one existing at a sharp leading edge at $x = 0$, which is known as the modified Blasius solution. The initial temperature profile is formed by assuming a generalized Crocco relationship between the velocity and the total enthalpy profiles. For the electron temperature profile, a constant electron temperature $[\theta_e(0, \eta) = T_e/T_{e_\infty} = 1]$ is assumed and similarly for the electron continuity equation $[n_e(0, \eta) = n_{e_s}(\infty)]$.

b. Turbulent flow

The initial velocity profile is taken to match up the classical turbulent $\frac{1}{7}$ power law velocity profile with a laminar sublayer, while for the temperature profile the Crocco relation is also used. For the electron temperature and concentration profiles, the best assumptions are the same ones used for the laminar flow.

4. Finite-Difference Procedure

The boundary-layer equations are replaced with implicit finite-difference equations in such a way that they are decoupled and written so that only one dependent variable appears in each equation. The nonlinear terms are linearized using the previous values. For accuracy and stability purposes, a prediction of the variables and the transport properties has been developed and a new iteration procedure has been used.

Results and Discussion

For the numerical results of both the infinite and finite rates of ionization, the following conditions have been used: 1) the plasma is initially composed of argon gas seeded with 1% by volume of cesium; 2) the magnetic field is constant along the channel, $B_z = 2$ Tesla; 3) the Hall parameter is assumed constant, $\beta = 2$. The initial thermodynamic conditions imposed on the channel are shown in Fig. 1.

The channel geometry is assumed to have an initial insulator length of 10 cm with no current or electric fields, followed by successive conductor and insulator pairs, where each is 3 cm long. Over the electrode, the thermionic emission (i) has been allowed to take its maximum value linearly over 2.5% of the conductor length. The current (j_{y_∞}) is assumed to take its maximum value at 97.5% of the conductor length. Finally, both emission and current density are allowed to fall off linearly in the remaining 2.5% of the conductor length.

The numerical calculations for turbulent flow were started at $x = 20$ cm. This starting point has been considered the beginning of the first electrode pair.

1. Infinite Rates of Ionization

Figures 2–4 represent some of the numerical results obtained for laminar flow where the maximum current density was 2000 amp/m^2, and the thermionic emission was 4000 amp/m^2. Figure 2 shows the variation of the electron wall temperature and sheath voltage drop along the channel for three successive pairs of insulator and conductor segments. The behavior of this curve over the insulator is related directly to the wall boundary

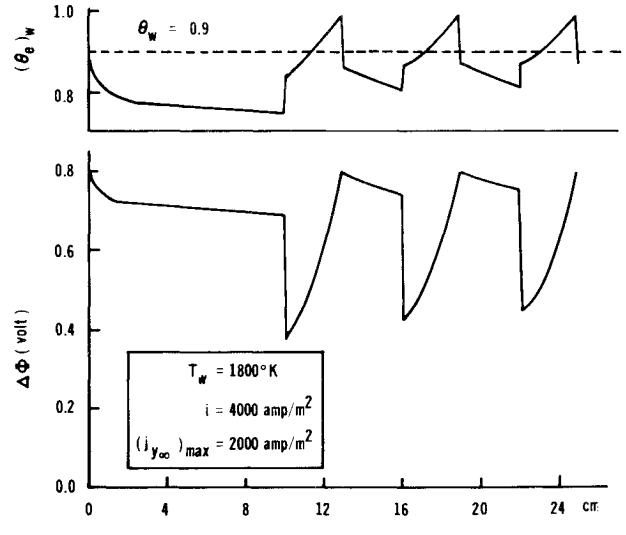

Fig. 2 Variation of electron wall temperature θ_{e_w} sheath voltage drop along the channel.

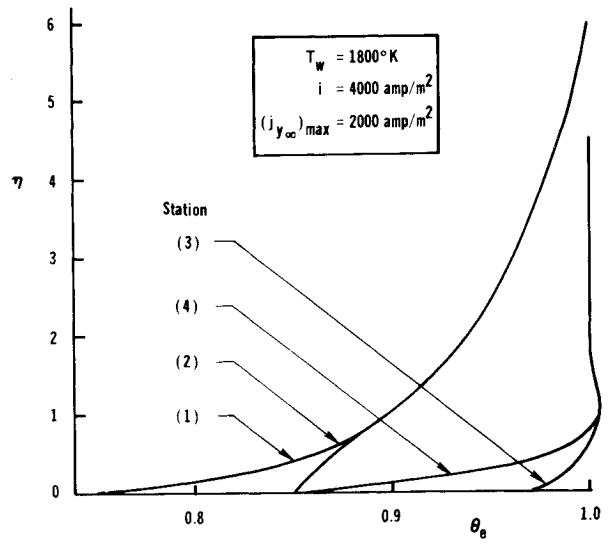

Fig. 3 Electron temperature profiles for the first electrode.

conditions, Eqs. (11) and (12). Over the conductor, three distinct different regions exist. First, as emission starts to build up, $\Delta\phi$ must decrease to allow for more electrons from the continuum regime to pass through the sheath to counteract the thermionic emission flux. This also affects the wall boundary condition for the electron temperature and causes a rise in it. In the second region where emission is constant and the current j_{y_∞} starts to climb, $\Delta\phi$ increases to satisfy the conservation of electrons. Also, because of the effect of joule heating $\theta_{e_w}(T_{e_w}/T_{e_\infty})$ increases. The electron wall temperature not only exceeds the surface temperature but also approaches the freestream temperature near the end of the conductor. In the third region, when both emission and current density are brought down to zero, the wall electron temperature derivative [Eq. (13)] will increase since both the cooling effect of thermionic emission and joule heating

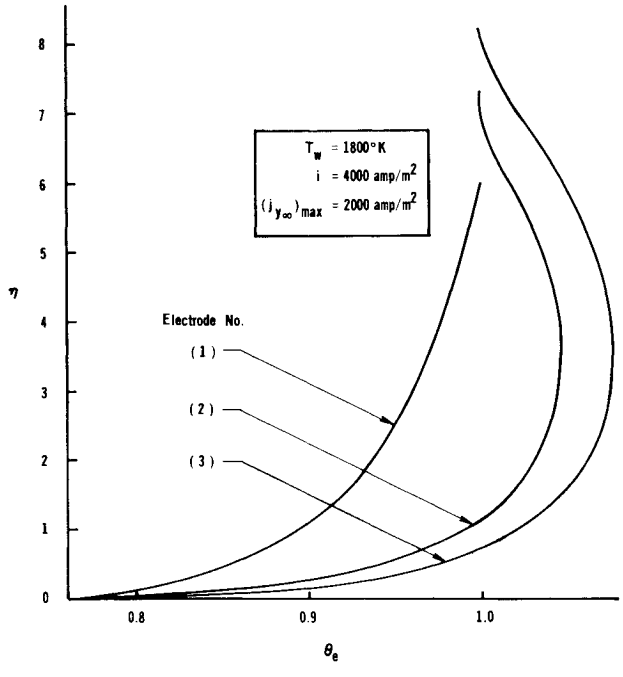

Fig. 4 Electron temperature profiles at the beginning of successive electrodes.

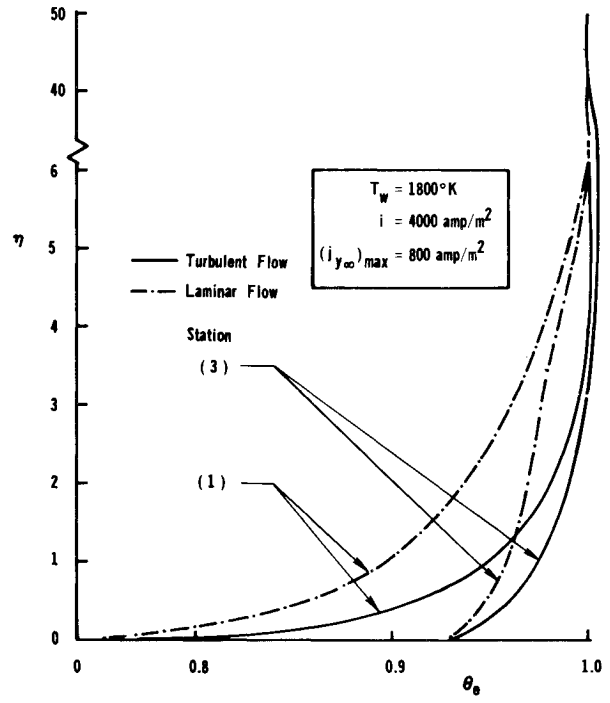

Fig. 5 Electron temperature profiles over the first electrode for laminar and turbulent flows.

disappears. This leads to a decrease in θ_{e_w}, while $\Delta\phi$ tends to increase more to cut off the electron flux.

Figure 3 illustrates the electron temperature profile across the boundary layer for four different locations (Fig. 1) along the conductor. At station 1, the end of the insulator segment, T_{e_w} is less than T_w. At station 2, after building up the emission current, only the region near the wall has been affected, because it is a sheath boundary condition change. The whole profile at station 3 has been shifted towards higher values because the joule heating is felt throughout the boundary layer, especially near the wall where σ is small. At the end of the conductor, station 4, the only change from the station 3 profile is again at the bottom of the boundary layer due to the change in the boundary condition.

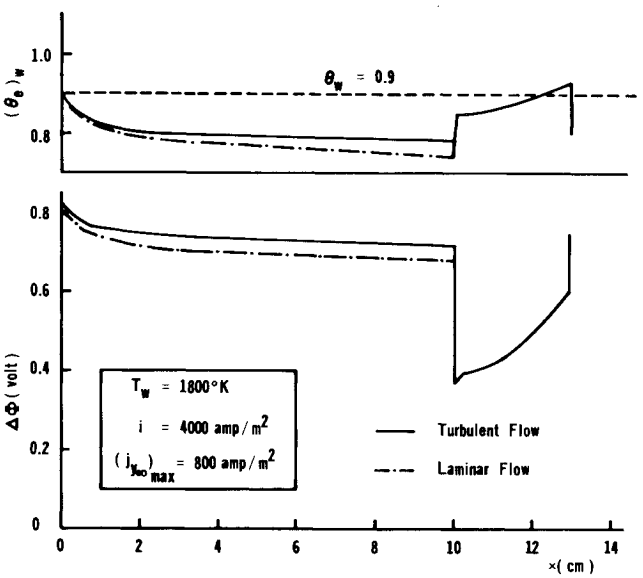

Fig. 6 Electron wall temperature and sheath voltage drop along the channel for laminar and turbulent flow.

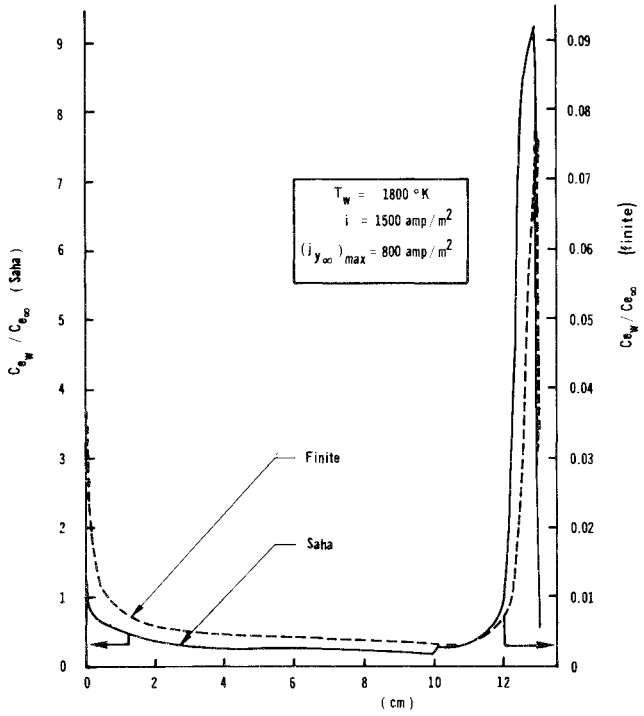

Fig. 7 Electron density ratio along the channel.

Figure 4 presents the electron temperature profiles at the beginning of successive electrodes. It shows clearly that these profiles are not similar. The history effect is very strong and is carried out along the channel. Any attempt to use a similar solution behavior will not show the present results.

Qualitatively, both laminar and turbulent flow results behave similarly. Figure 5 shows that the electron temperature profiles for turbulent flow are much fuller than the laminar flow profiles in the same way as the velocity and gas temperature profiles are, but for different reasons. This is not directly due to turbulence effect caused by the electron eddy transport coefficients, because the electron transport properties are negligibly affected by turbulence due to their high mobility. However, the differences are the result of two factors: a) more heat convection near the bottom of the boundary layer because of higher velocities for turbulent flow; and b) because the gas temperature profile is fuller for turbulent flow, the collision term will act in the same way to get the electron temperature to approach the gas temperature. For the same reason, the electron wall temperature for turbulent flow is higher than for laminar flow over the insulator (Fig. 6), while they are almost the same over the conductor because of the strong effect of joule heating. The sheath voltage drop follows the same trend as the electron wall temperature.

Other effects such as the influence of wall temperature (T_w), freestream current (j_{y_∞}) and thermionic emission (i) have been also examined and the results are listed in Ref. 15.

2. Finite Rate of Ionization

For this case, the finite electron number density is calculated independently using the electron continuity equation. The computational problems associated with the finite rate of ionization case are the same as the infinite case, but they are more serious.

Figures 7–9 represent some of the finite rate computational results for the laminar flow. Figure 7 illustrates the variation of the electron density ratio along the channel. It shows the big difference in magnitude between the finite and the equilibrium (Saha) electron number density at the wall. The "Saha" curve in this figure describes the equilibrium electron density ratio value obtained from the Saha equation at the local electron temperature for the finite rate case. Over the insulator there is a difference of about two orders of magnitude between the two quantities where the finite electron number density is the smaller. This happens because of the ambipolar diffusion near the wall, which has a strong effect of depleting the electrons from the bottom of the boundary layer. Over the conductor, three different regions are discussed separately. As emission builds up, the electron temperature rises and so does the equilibrium electron number density. On the other hand, the ambipolar diffusion is still very strong and almost no variation takes place in the finite number density. This leads to a large sheath voltage drop compared to the infinite rate case (see Fig. 12) in order to allow more electrons from the continuum regime to penetrate the sheath. When emission becomes constant and j_{y_∞} starts to increase, the effect of joule heating (j^2/σ) will be felt strongly through the boundary layer because of low σ. This will cause a pronounced increase in the electron temperature and hence the Saha electron number density. The electron production term depends on both the equilibrium and finite number densities, and for it to counteract the ambipolar diffusion term, both the actual and equilibrium electron densities should be high. Therefore, when the electron temperature climbs quickly, the finite rate term begins to be active and once this happens, the finite electron number density grows rapidly too. In the third region, as the emission and current density falls down at the end of the con-

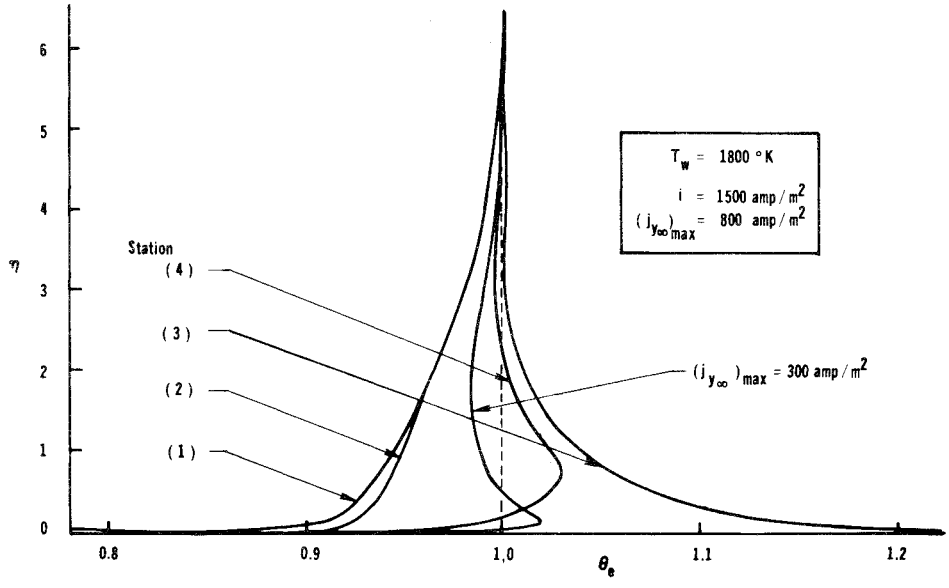

Fig. 8 Electron temperature profiles over the electrode.

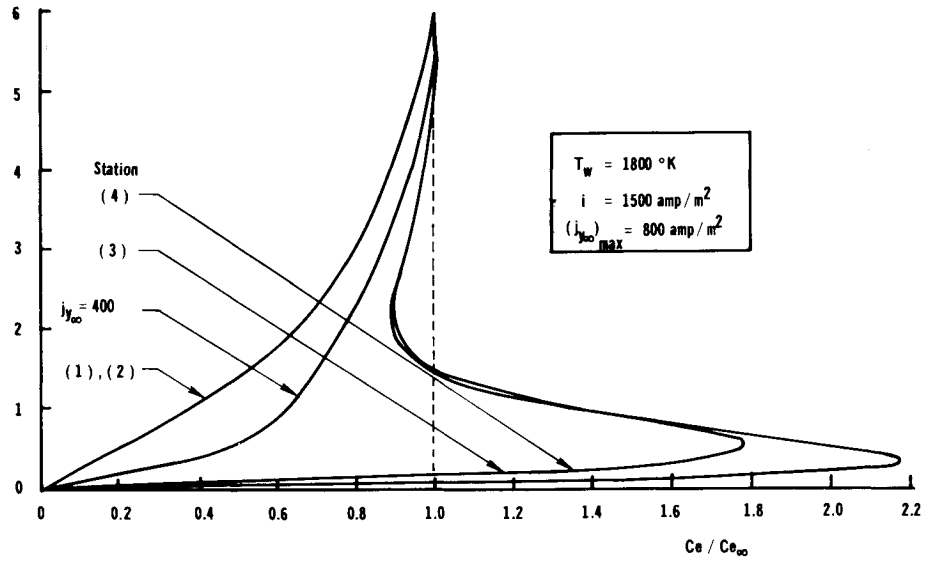

Fig. 9 Electron density ratio profiles over the electrode.

ductor, the electron temperature and densities fall down too. It should be noticed that the equilibrium number density of electrons goes down much faster than the actual finite number density which indicates (as expected) that the finite number density is always lagging behind in feeling any variations.

Figure 8 which exhibits the electron temperature profiles over the conductor, shows the effect of joule heating (j^2/σ) in raising the electron temperature across the boundary layer. Once more, this is a result of the small value of σ corresponding to the low electron density caused by ambipolar diffusion. One of the interesting results in this figure is that the electron temperature gradient at the wall changes its sign as j_{y_∞} increases (this means negative electron heat flux contribution to the wall). This can be explained by examining Eq. (12) for the electron temperature wall boundary condition. Because of the thermionic emission cooling effect and the pronounced increase in $\Delta\phi$ as j_{y_∞} grows, the net effect is for θ_{e_w}' to be negative, i.e., a cooling effect. [Note that $\Delta\phi$ appears with a negative sign in the exponent of the first term in the right-hand side of Eq. (12).] The equilibrium electron density ratio can be concluded from this figure using the Saha relation.

Figure 9 shows the actual finite rate density ratio profiles across the boundary layer and they can be explained with the following two points: 1) the ambipolar diffusion effect is felt mostly near the surface even when the current density j_{y_∞} increases; and 2) because of the extremely large values of the equilibrium electron number density (Saha) near the bottom of the boundary layer, the production term in the electron energy equation forces the finite number density to increase and even to overshoot to more than double the freestream value. As a result, ambipolar diffusion has two effects on the electron concentration at the conductor surface. The first is a direct effect, that is, a very low electron concentration at the wall. The other effect is a very high derivative of the electron concentration at the wall.

Figure 10 shows a comparison between the present results and those of Brown[7] for laminar flow at $x = 7.44$ cm. The calculations have been carried out for conditions similar to those of Brown while the freestream temperature was adjusted to take care of the radiation escape which is neglected in the present work. Besides the good agreement in the results, the effect of ambipolar diffusion is clearly shown here; the equilibrium

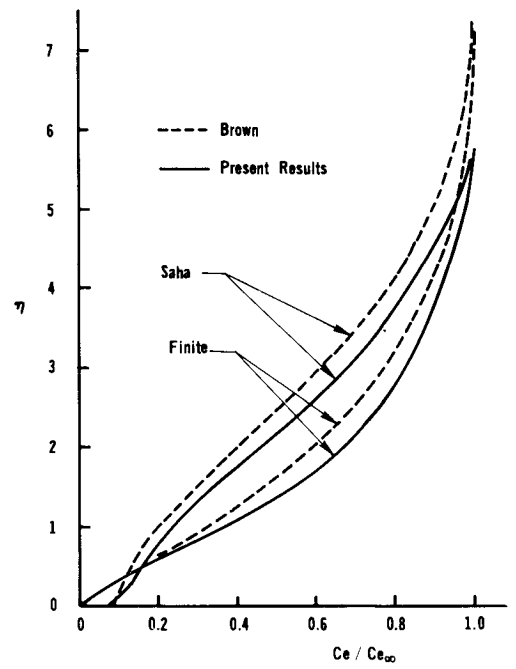

Fig. 10 Comparison results for the electron density ratio over the insulator.

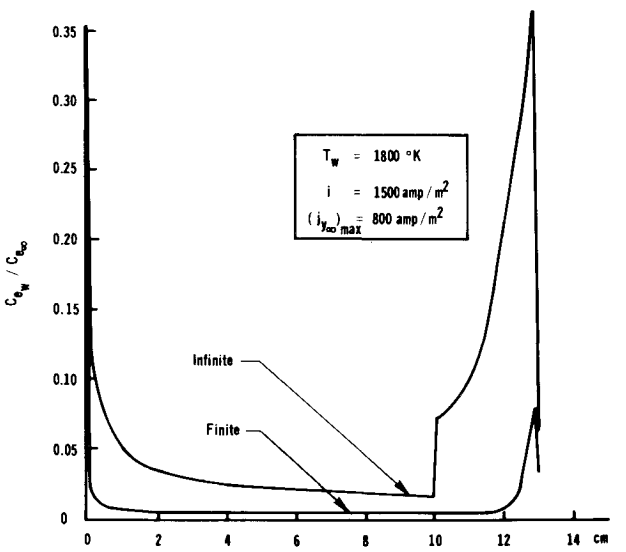

Fig. 11 Electron wall density ratio along the channel.

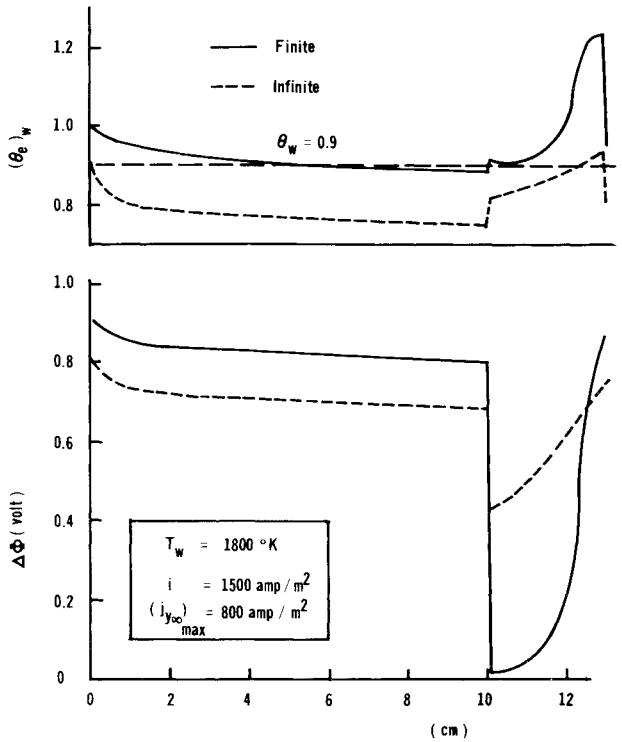

Fig. 12 Electron wall temperature and sheath voltage drop along the channel for finite and infinite rate (laminar flow).

density ratio at the wall is about 0.08 while it is almost zero (0.00011) for the finite rate case. Away from the wall, the ambipolar diffusion effect is weak and the finite curve overlaps the equilibrium curve until they approach each other near the edge of the boundary layer.

The turbulent flow results for the finite rate of ionization showed qualitatively similar results as the laminar flow. The reason for that and for the differences are the same ones mentioned for the infinite rates case (Figs. 5, 6).

3. Comparison between Finite and Infinite Rate of Ionization

When the analysis of the finite rate of ionization was studied earlier, the ambipolar diffusion was thought to be very small and was introduced in the equations just for completeness. However, the results showed that this is not true and its effect is very strong over both the insulator and conductor segments.

Figure 11 illustrates the behavior of the electron density ratio at the wall along the channel. The ambipolar diffusion term is responsible for depleting the number of electrons near the wall. Another observation is that when emission builds up, the infinite rate electron number density jumps up due to an increase in the electron wall temperature, while for the finite rate case, no such change takes place.

Figure 12 shows the variation of the electron wall temperature and sheath voltage drop along the channel. The following points are noticed: 1) over the insulator, the electron wall temperature is higher for the finite rates solution. This is also because of the ambipolar diffusion. The electron energy heat loss to the wall by conduction, $(k_e \partial T_e/\partial y)_w$, is much less for finite rates because of the very low value of k_{e_w} corresponding to the relatively low n_{e_w}. The variation of the sheath voltage drop follows the electron wall temperature and density behavior directly, and the result is a higher sheath voltage drop value for the finite rate case; and 2) over the conductor, because of low n_e for the finite rate solution, the thermionic emission has a bigger effect on the decrease of the value of the sheath voltage drop in order to allow for more electrons to pass through the sheath. That is why the value of 1500 amp/m^2 for the emission current has been used for the finite rate cases and is considered almost the maximum value without having a negative sheath voltage drop and a non-physical situation.

Figure 13 illustrates the electron density ratio profiles across the boundary layer at different locations over the conductor. The curves are shifted towards higher values for the finite rate solution except near the wall. Again the ambipolar diffusion is responsible for such a behavior.

Summary and Conclusion

There are major computational and physical conclusions that have been drawn out of the present work. The computational conclusions will not be listed here, despite their importance, and they are discussed in detail in Ref. 15. The major physical conclusions can be summarized as follows:

1) Complete solutions of the boundary-layer equations have been calculated over many electrode pairs for both laminar and turbulent flows.

2) Nonsimilar effects (history effect) are very strong and are exhibited in the solution.

3) Ambipolar diffusion, for the finite rate of ionization case, is very important. While its primary effect is to deplete the number of electrons near the wall, it is also felt strongly in the electron energy equations. Augmented joule heating and higher electron temperature are examples of such side effects.

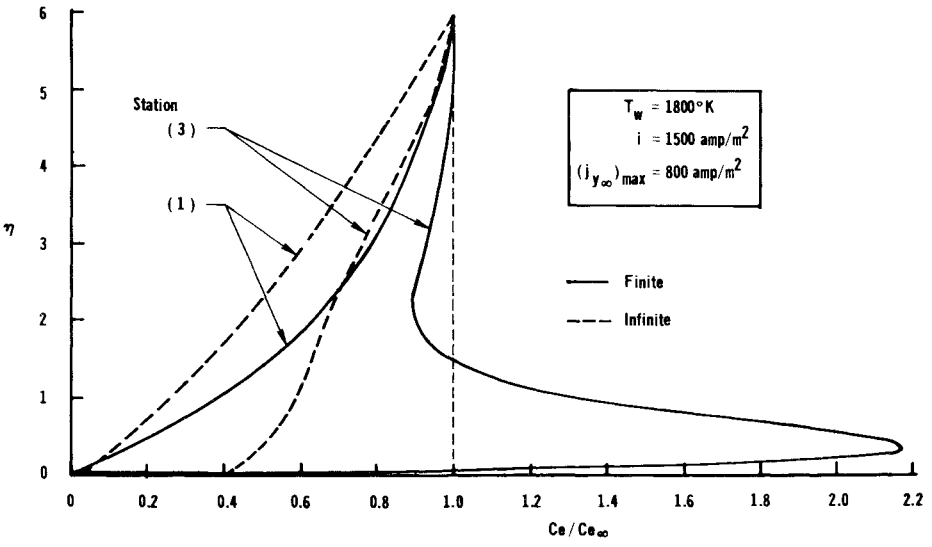

Fig. 13 Electron density ratio profiles over the conductor.

4) No special problems have been found in the solution of the turbulent flow equations. This is because the electron transport properties in the electron energy and electron continuity equation are negligibly affected by turbulence. However, the solution is different from that for the laminar flow because the convective and collision terms include the mean gas velocities and temperature which are all different depending on the type of flow.

5) Thermal nonequilibrium is strong near the wall over both the insulator and conductor segments.

6) A cooling effect takes place over the conductor for the finite rate case, where the electron temperature gradient changes its sign. This behavior is attributed also to the ambipolar diffusion.

References

[1] Kerrebrock, J. L., "Similar Solutions for Boundary Layers in Constant-Temperature Magneto-Gasdynamic Channel Flow," Readers' Reform, *Journal of the Aerospace Sciences,* Vol. 27, No. 2, Feb. 1960, pp. 156–157.

[2] Kerrebrock, J. L., "Electrode Boundary Layers in Direct-Current Plasma Accelerators," *Journal of the Aerospace Sciences,* Vol. 28, No. 8, Aug. 1961, pp. 631–640.

[3] Hale, F. J. and Kerrebrock, J. L., "Insulator Boundary Layers in Magneto-Hydrodynamic Channels," *AIAA Journal,* Vol. 2, No. 3, March 1964, pp. 461–469.

[4] Oates, G. C., Richmond, J. K., Aoki, Y., and Grohs, G., "Loss Mechanism of a Low Temperature Plasma Accelerator," *ARS Journal,* April 1962, pp. 541–548.

[5] Sherman, A. and Reshotko, E., "The Nonequilibrium Boundary Layer along a Channel Wall," AIAA Paper 68-134, Washington, D.C., 1968.

[6] Sherman, A., Yeh, H., Reshotko, E., and McAssey, E., Jr., "MHD Boundary Layers with Non-Equilibrium Ionization and Finite Rates," AIAA Paper 71-139, New York, 1971.

[7] Brown, R. T., "Electron Temperature and Number Density Measurements in a Nonequilibrium Plasma Boundary Layer," SU-IPR Rept. 350, Jan. 1970, Institute for Plasma Research, Stanford Univ., Stanford, Calif.

[8] Cott, D. W., "Ionizational and Electron Thermal Nonequilibrium in MHD Boundary Layers," *AIAA Journal,* Vol. 9, No. 12, Dec. 1971, pp. 2404–2410.

[9] Teno, J., Liu, C., and Brogan, T. R., "Boundary Layers in MHD Generators," *Proceedings of the 10th Symposium on the Engineering Aspects of MHD,* March 1969, MIT, Cambridge, Mass.

[10] Sonju, O. K., Teno, J., and Brogan, T. R., "Comparison of Experimental and Analytical Results for a 20 MW Combustion-Driven Hall Configuration MHD Generator," *Proceedings of the 11th Symposium on the Engineering Aspects of MHD,* California Inst. of Technology, Pasadena, Calif., March 1970.

[11] High, M. D. and Felderman, E. J., "Turbulent MHD Boundary Layers with Electron Thermal Nonequilibrium and Finite Rate Ionization," *AIAA Journal,* Vol. 10, No. 1, Jan. 1972, pp. 98–103.

[12] Demetriades, S. T., Argyropoulos, G. S., and Maxwell, C. D., "Progress in Analytical Modeling of MHD Power Generators," *Proceedings of the 12th Symposium on the Engineering Aspects of MHD,* Argonne National Lab., Argonne, Ill., March 1972.

[13] Argyropoulos, G. S., Demetriades, S. T., and Lackner, K., "Compressible Turbulent Magnetohydrodynamic Boundary Layers," *The Physics of Fluids,* Vol. 11, No. 12, Dec. 1968, pp. 2559–2566.

[14] Bird, R. B., Stewart, W. E., and Lightfoot, E. N., *Transport Phenomena,* Wiley, New York, 1960.

[15] Doss, E. D., "MHD Boundary Layers on a Segmented Electrode Wall of a Nonequilibrium Generator," Ph.D. Thesis, Sept. 1972, Univ. of California at Davis, Davis, Calif.

[16] Hinnov, E. and Hirschberg, J. G., "Electron-Ion Recombination in Dense Plasmas," *Physical Review,* Vol. 125, No. 3, Feb. 1962, pp. 795–801.

[17] Camac, M. and Kemp, N. H., "A Multitemperature Boundary Layer," Rept. 184, Aug. 1964, Avco Everett Research Lab., Everett, Mass.

[18] Rosa, R. J., *Magnetohydrodynamic Energy Conversion,* McGraw-Hill, New York, 1968.

[19] Cebeci, T., "Calculation of Compressible Turbulent Boundary Layers with Heat and Mass Transfer," *AIAA Journal,* Vol. 9, No. 6, June 1971, pp. 1091–1097.